Hindawi
International Journal of Antennas and Propagation
Volume 2022, Article ID 6856050, 10 pages
https://doi.org/10.1155/2022/6856050

Research Article

Fast Tensor-Based Joint Estimation for Time Delay and Angle of Arrival in OFDM System

Jinzhi Du, Weijia Cui, Bin Ba, Chunxiao Jian, and Haiyun Xu

National Digital Switching System Engineering & Technological Research Center, Zhengzhou 450001, Henan Province, China

Correspondence should be addressed to Jinzhi Du; dujinzhi0811@163.com

Received 11 April 2022; Revised 27 August 2022; Accepted 19 September 2022; Published 27 September 2022

Academic Editor: Hervé Aubert

Nowadays, the joint estimation of time delay (TD) and angle of arrival (AOA) using conventional vector structure suffers from the considerable complexity of multidimensional spectrum search. Therefore, a fast estimation method using orthogonal frequency division multiplexing (OFDM) technology and uniform planar array (UPA) is proposed in this paper, which adopts low-complexity tensor-based operations and spatial-frequency features to reconfigure the channel frequency response. To begin with, the array response is integrated with the OFDM signal characteristics to build an extended array in tensor form. Afterwards, we process the covariance matrix of the tensor structure by CANDECOMP/PARAFAC decomposition (CPD) to separate the respective signal subspaces of TD and AOA estimates. Finally, we conduct a one-dimensional (1-D) spectrum search to locate the TD estimates and a two-dimensional (2-D) spectrum search to locate the AOA estimates. The simulated performance demonstrates that the proposed algorithm offers precise estimates at low signal-to-noise ratios in a multipath environment and outperforms traditional vector-based algorithms with respect to computational complexity.

1. Introduction

Orthogonal frequency division multiplexing (OFDM), a multicarrier digital modulation technique, uses multiple parallel subcarriers to achieve serial high-rate data communication. The subcarriers are orthogonal to each other, which can combat frequency-selective fading in an effective way. Moreover, the OFDM system can offer data traffic and positioning services to users, which are extensively applied in 5G mobile communication [1], IEEE 802.11 protocol [2], satellite communication [3], intelligence steer [4], and underwater acoustic communication [5]. Time delay (TD) and angle of arrival (AOA) are significant factors for positioning systems, as for indoor localization [6] and radar [7]. The frequency-domain AOA estimation algorithm [8] is studied with the same multiple signal classification (MUSIC) approach as the time-domain narrowband signal model. However, its capability is limited due to the size of the array aperture. The algorithm in [9] proposes a TD estimation method for OFDM signals, but this algorithm is not available in multipath environments. As researchers choose super-resolution approaches like MUSIC [10], estimating signal parameters via the rotational invariance techniques (ESPRIT) [11], the propagator method (PM) [12], and compressive sensing [13], it is difficult for them to enhance the estimation accuracy due to the restrictions of the signal bandwidth.

The joint estimation of TD and AOA with spatio-time parameter coupling characteristics not only increase the accuracy but also decrease the amount of receiving nodes, thus reducing the system overhead and improving the efficiency of the positioning system. Hence, the joint estimation methods employed are important. In addition, a method presented in [14] solves TD under wideband signal conditions and then estimates AOA according to the triangular geometry with TD inequality, but its performance is not significantly improved. In further, a method for constructing an extended channel frequency response to obtain highly accurate joint estimation using an OFDM system is proposed in [15]. Nevertheless, the complexity of the method is extremely high due to the need for full-field-of-view search.

Tensor as an efficient way to process multidimensional data have achieved extensive research and applications in fields such as machine learning [16], image processing [17], MIMO radar [18], and vehicle-to-everything communication [19]. Unlike traditional vector bases, tensor processing, with the help of data Kronecker structural properties, breaks up large-scale matrix operations into multiple small-scale matrix operations, avoiding additional overhead due to repeated calculations.

Most of the above algorithms use uniform linear arrays (ULA) [20] for parameter estimation. Due to the one-dimensional (1-D) structure, only azimuthal angles can be estimated, and two-dimensional (2-D) angle search cannot be achieved. This paper studies the joint estimation for TD and AOA of OFDM techniques under uniform planar arrays (UPA) [21], which are commonly used in practical engineering to obtain stable 2-D angle estimates.

Furthermore, we propose a joint estimation algorithm for multipath environments that functions to keep the estimation precision highly while reducing the considerable complexity associated with spectrum peak search methods. The channel frequency response of multiple subcarriers of the OFDM signal combined with the array response of the receiving antenna can be applied to construct an extended virtual array response with accurate estimation. We reconfigure the extended virtual array response by taking advantage of the structure of the tensor structure, which reduces the spectrum peak search dimension while maintaining the original estimation accuracy. Moreover, we can estimate TD and AOA separately, which greatly reduces the complexity.

The rest of the paper is summarized as follows. At first, we introduce the signal model and the corresponding joint estimation algorithm applied to the vector-based algorithm in Section 2. In Section 3, we describe the transformation of the signal model under a tensor structure and the corresponding joint estimation algorithm and further outline the algorithm procedure. We perform the complexity analyses in Section 4. For Section 5, we analyze the simulation performance. In the end, we summarize our efforts in Section 6. The notations used in this paper are described in Table 1.

Table 1: Notations.

Identity matrix	I
Transpose	$(\bullet)^T$
Conjugate	$(\bullet)^*$
Hermitian transpose	$(\bullet)^H$
Kronecker product	$\otimes$
Khatri-rao product	$\odot$
Tensor outer product	$\circ$
Orthogonalization	$\mathrm{orth}[\bullet]$
Statistical expectation	$E\{\bullet\}$
Tensor contraction along the qth dimension	$\langle \bullet, \bullet \rangle_{\{q\}}$

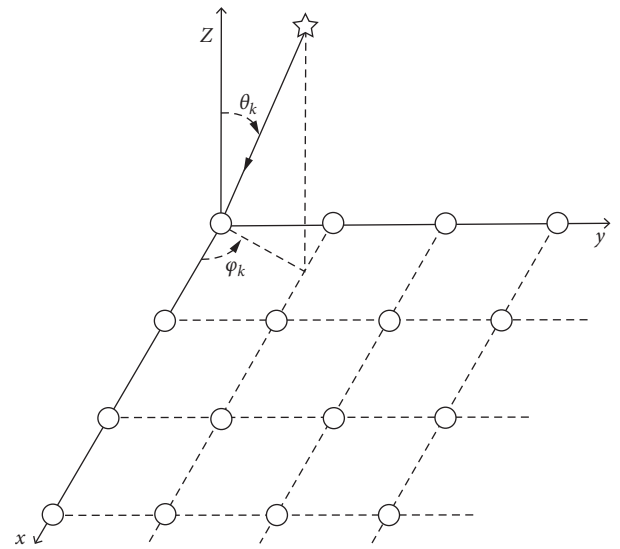

Figure 1: Signal arrives in UPA.

2. Vector-Based Algorism

2.1. Signal Model. The array sensors used in this paper consist of $M \times M$ array sensors as illustrated in Figure 1. The function of this model is to estimate TD and AOA without needing to set the signal source position. Scholars typically model multipath wireless propagation channels typically as complex low-pass equivalent impulse responses. Following channel estimation, the channel impact response of the array sensor at location (x, y) in the sth snapshot is denoted as follows:where K indicates the quantity of multipaths, $\alpha_k^{(s)} e^{j\beta_k^{(S)}}$ is the complex attenuation in the kth path, $\alpha_k^{(s)}$ is its amplitude, $\beta_k^{(s)}$ is its phase, which matches the uniform distribution with density function $U(0, 2\pi)$.

$$h_{x,y}^{(s)}(t) = \sum_{k=1}^{K} \alpha_k^{(s)} e^{j\beta_k^{(s)}} \delta\left(t - \tau_k - \xi_{k,x,y}\right), \tag{1}$$

We assume that the reference array sensor is the array sensor at the origin of the coordinate axis. In the multipath environment, the propagation delay of the signal source reaching the reference array sensor via the kth path is τ_k. And, the relative delay of the array sensor at (x, y) is $\xi_{k,x,y}$, denoted as follows:

$$\xi_{k,x,y} = \frac{\lambda \sin \theta_k \left(x \cos \varphi_k + y \sin \varphi_k\right)}{2c}, \tag{2}$$

In which λ is the impinging signal wavelength; (φ_k, θ_k) is the direction of the incident signal.

We assume that the quantity of OFDM subcarriers is L. After the Fourier transform of (1), the channel frequency domain response for the lth subcarrier at the (x, y) array sensor can be obtained as follows:

$$H_{l,x,y}^{(s)} = \sum_{k=1}^{K} \alpha_k^{(s)} e^{j\beta_k^{(s)}} e^{-j2\pi\left(f_c + \Delta f l\right)\left(\tau_k + \xi_{k,x,y}\right)} + n_{l,x,y}^{(s)}, \tag{3}$$

where Δf is the subcarrier spacing, f_c is the carrier frequency, and $n_{l,x,y}^{(s)}$ is additive white Gaussian noise at power σ^2. From (3), the channel frequency response for lth subcarrier is obtained as follows:

$$\mathrm{H}_l^{(s)} = \begin{bmatrix} H_{l,0,0}^{(s)} \\ H_{l,0,1}^{(s)} \\ \vdots \\ H_{l,M-1,M-1}^{(s)} \end{bmatrix} = \mathrm{A}_l(\boldsymbol{\tau}, \boldsymbol{\xi})\boldsymbol{\rho}^{(s)} + \mathrm{n}_l^{(s)}, \tag{4}$$

where

$$\begin{aligned} \tau &= \left[\, \tau_1 \;\; \tau_2 \;\; \cdots \;\; \tau_K \,\right]^T, \\ \xi &= \left[\, \xi_1 \;\; \xi_2 \;\; \cdots \;\; \xi_K \,\right], \\ \xi_k &= \left[\, \xi_{k,0,0} \;\; \xi_{k,0,1} \;\; \cdots \;\; \xi_{k,M-1,M-1} \,\right]^T, \\ \rho_k^{(s)} &= \alpha_k^{(s)} e^{j\beta_k^{(s)}}, \\ \rho^{(s)} &= \left[\, \alpha_1^{(s)} e^{j\beta_1^{(s)}} \;\; \alpha_2^{(s)} e^{j\beta_2^{(s)}} \;\; \cdots \;\; \alpha_k^{(s)} e^{j\beta_k^{(s)}} \,\right]^T, \\ A_l(\tau, \xi) &= \left[\, a_l(\tau_1, \xi_1) \;\; \cdots \;\; a_l(\tau_K, \xi_K) \,\right], \\ a_l(\tau_k, \xi_k) &= \left[\, a_l\left(\tau_k, \xi_{k,0,0}\right) \;\; \cdots \;\; a_l\left(\tau_k, \xi_{k,M-1,M-1}\right) \,\right]^T. \end{aligned} \tag{5}$$

In which $a_l(\tau_k, \xi_{k,x,y}) = e^{-j2\pi(f_c + \Delta f l)(\tau_k + \xi_{k,x,y})}$, and

$$n_l^{(s)} = \left[\, n_{l,0,0}^{(s)} \;\; n_{l,1,0}^{(s)} \;\; \cdots \;\; n_{l,M-1,M-1}^{(s)} \,\right]^T. \tag{6}$$

In case there are a total of S snapshots, (4) is denoted by the following equation:

$$\mathrm{H}_l = \mathrm{A}_l(\boldsymbol{\tau}, \boldsymbol{\xi})\boldsymbol{\rho} + \mathbf{n}_l, \tag{7}$$

where

$$\begin{aligned} \boldsymbol{\rho} &= \left[\, \boldsymbol{\rho}^{(1)} \;\; \boldsymbol{\rho}^{(2)} \;\; \cdots \;\; \boldsymbol{\rho}^{(S)} \,\right], \\ \mathrm{n}_l &= \left[\, \mathrm{n}_l^{(1)} \;\; \mathrm{n}_l^{(2)} \;\; \cdots \;\; \mathrm{n}_l^{(S)} \,\right]. \end{aligned} \tag{8}$$

According to the space-time equivalence, OFDM signal subcarriers can be analogous to the array sensors. Based on the space signal processing algorithm, an extended channel frequency response (EX-Response) matrix $\mathrm{H} \in \mathbb{C}^{M^2 L \times S}$ with coupled spatial-frequency information can be constructed whose expression is

$$\mathrm{H} = \begin{pmatrix} \mathrm{H}_0 \\ \mathrm{H}_1 \\ \vdots \\ \mathrm{H}_{L-1} \end{pmatrix} = \begin{pmatrix} \mathrm{A}_0(\boldsymbol{\tau}, \boldsymbol{\xi}) \\ \mathrm{A}_1(\boldsymbol{\tau}, \boldsymbol{\xi}) \\ \vdots \\ \mathrm{A}_{L-1}(\boldsymbol{\tau}, \boldsymbol{\xi}) \end{pmatrix} \boldsymbol{\rho} + \mathrm{N} = \mathrm{A}(\boldsymbol{\tau}, \boldsymbol{\xi})\boldsymbol{\rho} + \mathrm{N}, \tag{9}$$

where

$$\mathrm{N} = \left(\, \mathrm{n}_0^T \;\; \mathrm{n}_1^T \;\; \cdots \;\; \mathrm{n}_{L-1}^T \,\right)^T. \tag{10}$$

The model converts the time domain information to the frequency domain for processing and has the same structure as the traditional time domain narrowband model. In addition, building an EX-Response has two obvious merits. On the one hand, the virtual bandwidth is enlarged to M^2 multiples of the actual bandwidth. On the other hand, the virtual aperture is enlarged to L multiples of the actual aperture. From the perspective of parameter estimation, the bandwidth and aperture expansion will improve the performance of estimating TD and AOA.

2.2. The Joint TD and AOA Estimation. Combining (9), the covariance matrix can be defined for;

$$\mathrm{R}_H = \frac{1}{S}\mathrm{H}\mathrm{H}^H = \mathrm{A}(\boldsymbol{\tau}, \boldsymbol{\xi})\mathrm{R}_\rho \mathrm{A}(\boldsymbol{\tau}, \boldsymbol{\xi})^H + \sigma^2 \mathrm{I}_{M^2 L}, \tag{11}$$

where R_ρ is a complex attenuation covariance matrix. When the complex attenuations are independent, $\mathrm{rank}(\mathrm{R}_\rho) = K$. Due to $\mathrm{rank}(\mathrm{A}(\tau, \xi)) = K$ and $\mathrm{rank}(\mathrm{A}(\tau, \xi)\mathrm{R}_\rho \mathrm{A}(\tau, \xi)^H) = K$, the situation satisfies the requirements for using the MUSIC method. Furthermore, the eigenvalue decomposition of R_H can be expressed as follows:

$$\mathrm{R}_H = \mathrm{U}_S \boldsymbol{\Sigma}_S \mathrm{U}_S^H + \mathrm{U}_N \boldsymbol{\Sigma}_N \mathrm{U}_N^H, \tag{12}$$

where $\Sigma_N = \sigma^2 \mathrm{I}_{M^2 - K}$ is a diagonal matrix of $M^2 - K$ eigenvalues, and U_N is the noise subspace. Therefore, the joint estimated spatial spatial expression is expressed as follows:

$$P(\tau, \theta, \varphi) = \left\| \mathrm{U}_N^H \mathrm{A}(\tau, \xi) \right\|_2^{-2}. \tag{13}$$

Although $(\widehat{\tau}, \widehat{\theta}, \widehat{\varphi})$ is obtained by the three-dimensional (3-D) MUSIC approach with excellent estimation accuracy, the 3-D spectral peak search complexity is unacceptably high.

3. Tensor-Based Algorism

3.1. Signal Model. In the joint direction matrix $\mathrm{A}(\tau, \xi)$ of the vector basis, the propagation delay phase and the relative delay phase are stacked on the matrix columns by the Kronecker product, which are $M^2 L \times K$ dimensional matrices. The covariance matrix R_H generated by $\mathbf{A}(\tau, \xi)$ contains a large number of redundant terms, which imposes a serious computational burden on the 3-D spectrum peak search. In tensor operations, the large-scale matrix computation is decomposed into small-scale matrix computation, thus considerably reducing the computational load. In order to preserve the spatial-frequency characteristics of the EX-Response, the S snapshots are connected along the time dimension to form a 3-D tensor. Thus the tensor equivalent $\mathscr{H} \in \mathbb{C}^{M^2 \times L \times S}$ of (9) is

$$\begin{aligned} \mathscr{H} &= \mathbf{A}(\boldsymbol{\tau}, \boldsymbol{\xi}) \circ \boldsymbol{\rho}^{\mathrm{T}} + \mathscr{N} \\ &= \mathscr{V} \circ \mathbf{T} \circ \boldsymbol{\rho}^{\mathrm{T}} + \mathscr{N}, \end{aligned} \tag{14}$$

where.

$$\mathbf{T}_k = \begin{pmatrix} e^{-j2\pi f_c \tau_k} \\ e^{-j2\pi\left(f_c + \Delta f\right)\tau_k} \\ \vdots \\ e^{-j2\pi\left(f_c + \Delta f(l-1)\right)\tau_k} \end{pmatrix} \odot \begin{pmatrix} e^{-j2\pi\Delta f(0)\xi_{k,0,0}} \\ e^{-j2\pi\Delta f(1)\xi_{k,0,1}} \\ \vdots \\ e^{-j2\pi\Delta f(l-1)\xi_{k,M-1,M-1}} \end{pmatrix}, \tag{15}$$

$$\mathbf{T} = \left[\, \mathbf{T}_1 \;\; \mathbf{T}_2 \;\; \cdots \;\; \mathbf{T}_K \,\right].$$

Considering the practical situation, the relative time is considerably less compared to the propagation delay, and the subcarrier relative delay is even smaller, which means that it can be neglected. Thus, the equation can be established as follows:

$$\begin{aligned}\mathscr{T}_k &= \left[\, e^{-j2\pi f_c \tau_k} \;\; e^{-j2\pi (f_c+\Delta f)\tau_k} \;\; \cdots \;\; e^{-j2\pi (f_c+\Delta f(l-1))\tau_k} \,\right]^{\mathrm{T}} \\ &\approx \mathbf{T}_k, \\ \mathscr{T} &= \left[\, \mathscr{T}_1 \;\; \mathscr{T}_2 \;\; \cdots \;\; \mathscr{T}_K \,\right] \approx \mathbf{T}.\end{aligned} \tag{16}$$

Therefore, in order to separate the propagation time delay phase from the relative time delay phase, (3) can be approximated as follows:

$$\mathscr{H} \approx \mathscr{V} \circ \mathscr{T} \circ \boldsymbol{\rho}^{\mathrm{T}} + \mathscr{N}, \tag{17}$$

where

$$\begin{aligned}\mathscr{V}_k &= \left[\, e^{-j2\pi f_c \xi_{k,0,0}} \;\; e^{-j2\pi f_c \xi_{k,0,1}} \;\; \cdots \;\; e^{-j2\pi f_c \xi_{k,M-1,M-1}} \,\right]^{T}, \\ \mathscr{V} &= \left[\, \mathscr{V}_1 \;\; \mathscr{V}_2 \;\; \cdots \;\; \mathscr{V}_K \,\right],\end{aligned} \tag{18}$$

In which $\mathscr{N}$ is additive white Gaussian noise in the same dimension as $\mathscr{H}$ with power of σ^2.

3.2. The Joint TD and AOA Estimation. In (17), the tensor covariance matrix $\mathscr{R}_{\mathscr{H}} \in \mathbb{C}^{M^2\times L\times M^2\times L}$ can be obtained as follows:

$$\begin{aligned}\mathscr{R}_{\mathscr{H}} &= E\left[\langle \mathscr{H}, \mathscr{H}^* \rangle_{\{3\}}\right] \\ &= \sum_{k=1}^{K} \beta_k^2 \mathscr{V}_k \circ \mathscr{T}_{\mathrm{k}} \circ \mathscr{V}_{\mathrm{k}}^* \circ \mathscr{T}_{\mathrm{k}}^* + \mathscr{N}_{\mathscr{R}},\end{aligned} \tag{19}$$

where $\beta_k^2 = E[\rho_k^T (\rho_k^T)^*]$ is the complex decay of the kth path and $\rho_k = \left[\, \rho_k^{(1)} \;\; \rho_k^{(2)} \;\; \cdots \;\; \rho_k^{(S)} \,\right]$; $\mathscr{N}_{\mathscr{R}} = \mathrm{E}[\langle \mathscr{N}, \mathscr{N}^* \rangle_{\{3\}}]$ is the noise term. In practice, the tensor covariance matrix $\mathscr{R}_{\mathscr{H}}$ can be estimated as follows:

$$\widehat{\mathscr{R}}_{\mathscr{H}} = \frac{1}{S} \langle \mathscr{H}, \mathscr{H}^* \rangle_{\{3\}}. \tag{20}$$

The CANDECOMP/PARAFAC decomposition (CPD) [22] is a common method for splitting a high-dimensional tensor. We perform CPD on the four-dimensional tensor $\widehat{\mathscr{R}}_{\mathscr{H}}$ to obtain a sum $\mathscr{R}_{CP} \in \mathbb{C}^{M^2\times K, L\times K, M^2\times K, L\times K}$ of component rank-one tensors as follows:

$$\mathscr{R}_{CP} = [\mathscr{V}_{CP}], [\mathscr{T}_{CP}], [\mathscr{V}_{CP}^*], [\mathscr{T}_{CP}^*]. \tag{21}$$

While the complex attenuations are independent, then there is

$$\begin{aligned}&\mathrm{rank}(\mathscr{V}_{CP}) + \mathrm{rank}(\mathscr{T}_{CP}) + \mathrm{rank}(\mathscr{V}_{CP}^*) \\ &\quad + \mathrm{rank}(\mathscr{T}_{CP}^*) \geq 2K + N - 1.\end{aligned} \tag{22}$$

Furthermore, the uniqueness of the CPD is satisfied [22], where N is the number of matrices obtained by the CPD or the dimension of the decomposed matrix. We extract the signal subspace $\mathscr{T}_{CP}$ from $\mathscr{R}_{CP}$ for TD estimation and the signal subspace $\mathscr{V}_{CP}$ for AOA estimation.

3.2.1. TD Estimation. We obtain the noise subspace $\mathbf{U}_{nt}\mathbf{U}_{nt}^H$ for TD estimation from the orthogonal complementary subspace of the signal subspace $\mathscr{T}_{CP}$ as follows:

$$\mathbf{U}_{nt}\mathbf{U}_{nt}^H = \mathbf{I} - \mathrm{orth}(\mathscr{T}_{CP})\mathrm{orth}(\mathscr{T}_{CP})^H. \tag{23}$$

Then, the spatial spectrum expression of the TD estimate can be obtained as follows:

$$P(\tau) = \frac{1}{\mathscr{T}(\tau)^H \left(\mathbf{U}_{nt}\mathbf{U}_{nt}^H\right)\mathscr{T}(\tau)}. \tag{24}$$

When $K < L$, we adopt the 1-D MUSIC method to obtain the $\widehat{\tau}$ value, which has a higher estimation accuracy and greatly reduces the computational complexity compared to the 3-D algorithm.

3.2.2. AOA Estimation. We obtain the noise subspace $\mathbf{U}_{na}\mathbf{U}_{na}^H$ for AOA estimation from the orthogonal complementary subspace of the signal subspace $\mathscr{V}_{CP}$ as follows:

$$\mathbf{U}_{na}\mathbf{U}_{na}^H = \mathbf{I} - \mathrm{orth}(\mathscr{V}_{CP})\mathrm{orth}(\mathscr{V}_{CP})^H. \tag{25}$$

Then, the spatial spectrum expression of the AOA estimate can be obtained as follows:

$$P(\theta, \varphi) = \frac{1}{\mathscr{V}(\theta, \varphi)^H \left(\mathbf{U}_{na}\mathbf{U}_{na}^H\right)\mathscr{V}(\theta, \varphi)}. \tag{26}$$

When $K < M$, we use the 2-D MUSIC method to obtain the $(\widehat{\theta}, \widehat{\varphi})$ value, which has a higher estimation accuracy and greatly reduces the computational complexity compared to the 3-D algorithm.

3.2.3. Algorithm Steps. Table 2 lists the main processes of the proposed algorithm.

4. Algorithm Complexity Analysis

This section analyzes the complexity of the proposed tensor-based algorithm (EX-Proposed) under the EX-Response model and compares it with the corresponding vector-based algorithm (EX-Vector-Based). For the simulation comparison in V, the complexity of the tensor-based algorithm (Proposed) and the corresponding vector-based algorithm (Vector-Based) employing a single-frequency model [8] is also compared.

The complexity of the algorithms can be split into vector-based covariance matrix computation, tensor-based covariance matrix computation, eigenvalue decomposition, CPD, and 1-D spectrum peak search, which are $\mathcal{O}(SM^4L^2)$, $\mathcal{O}(SM^4L)$, $\mathcal{O}(M^6L^3)$, $\mathcal{O}(2^NKM^4L^2 + NK^3)$, and $\mathcal{O}(M^2L(M^2L-K)G)$, separately, in which G represents the number of spectrum points in the 1-D search. Therefore, the complexity of the EX-Proposed is $\mathcal{O}(M^4L(S + 2^NKL) + NK^3 + M^2L(M^2L-K)(G_\varphi G_\theta + G_\tau))$. The cost of the EX-Vector-Based is $\mathcal{O}((S + M^2L)M^4L^2 + M^2L(M^2L-K)G_\varphi G_\theta G_\tau)$, in which G_φ, G_θ and G_τ indicate the quantity of searches for azimuth, elevation, and propagation delay, separately. Furthermore, the complexity of the single-frequency model

Table 2: Algorithm steps.

step1:	The tensor EX-Response matrix $\mathscr{H}$ is constructed according to (26).
step2:	The tensor covariance matrix $\widehat{\mathscr{R}}_{\mathscr{H}}$ is constructed based on (30).
step3:	Perform a CPD of $\widehat{\mathscr{R}}_{\mathscr{H}}$, which solves the signal subspaces $\mathscr{T}_{CP}$ and $\mathscr{V}_{CP}$, and then the corresponding noise subspaces and are obtained by (33) and (35), respectively. $\mathbf{U}_{nt}\mathbf{U}_{nt}^H$ and $\mathbf{U}_{na}\mathbf{U}_{na}^H$.
step4:	Proceeded to conduct a 1-D spectrum peak search for $\mathbf{U}_{nt}\mathbf{U}_{nt}^H$ to solve the $\widehat{\tau}$ by (34), and a 2-D spectrum peak search for $\mathbf{U}_{na}\mathbf{U}_{na}^H$ to solve the $(\widehat{\theta},\widehat{\varphi})$ by (36).

algorithms, i.e., Proposed and Vector-Based are $\mathcal{O}(M^4(SL + 2^N K) + NK^3 + M^2(M^2 - K)(G_\varphi G_\theta + G_\tau))$ and $\mathcal{O}((SL + M^2)M^4 + M^2(M^2 - K)G_\varphi G_\theta G_\tau)$, separately. In order to compare clearly, Table 3 summarizes the complexity of all methods. Furthermore, the complexity of the algorithms are compared in terms of snapshots (S), the number of sensors (M) , and the searching step ($\Delta\tau$ and $\Delta\varphi = \Delta\theta$, where $G_\varphi = 360/\Delta\varphi$, $G_\theta = 90/\Delta\theta$) in Figure 2(a)–2(d), respectively. For correspondence with subsequent simulations, we set $L = 64$, $K = 3$, and $N = 4$. The other parameters are described in Figure 2.

From Figure 2, the complexity of EX-Vector-based and Vector-based are extremely high due to the huge number of spectrum points, particularly in the condition of small spectrum steps. In contrast, tensor-based Proposed and EX-Proposed use CPD to handle the covariance matrix for reducing the dimensionality of the spectrum peak search. Thus, both methods significantly decrease the complexity. In contrast to the Proposed method, EX-Proposed adopts an EX-Response model, which has higher complexity and better estimation accuracy.

5. Simulation Results

This section performs a simulation experiment analysis in which the proposed tensor-based algorithm is compared with the vector-based algorithm. Furthermore, the improved algorithm using the EX-Response model is also compared with the corresponding vector-based algorithm. The Cramer–Rao bound (CRB) [23] is a threshold for the unbiased estimation variance of the proposed model and can be used as a performance reference benchmark.

Firstly, we assume that the parameter estimates are all performed individually with S snapshots, so the joint probability density function is expressed as follows:

$$f(\mathbf{H}(1),\ldots,\mathbf{H}(S)) = \frac{1}{(2\pi)^{M^2LS}\left(\sigma^2/2\right)^{M^2LS}} e^{-\left(1/\sigma^2\right)\sum_{s=1}^{S}(\mathbf{H}(s)-\mathbf{A}\boldsymbol{\rho}(s)^{\mathrm{H}}(\mathbf{H}(s)-\mathbf{A}\boldsymbol{\rho}(s))}. \tag{27}$$

Then, taking the log-likelihood function of (25), we obtain the following equation:

$$Lo(\mathbf{H}(1),\ldots,\mathbf{H}(S)) = -M^2LS\ln(2\pi) - M^2LS\ln\left(\sigma^2/2\right) - \frac{1}{\sigma^2}\sum_{s=1}^{S}(\mathbf{H}(s) - \mathbf{A}\boldsymbol{\rho}(s)^{\mathrm{H}}(\mathbf{H}(s) - \mathbf{A}\boldsymbol{\rho}(s)). \tag{28}$$

Define $\eta = [\tau^T, \theta^T, \varphi^T]^T$. In addition, $\widetilde{\rho}(s)$ and $\overline{\rho}(s)$ are the imaginary part and real part of $\rho(s)$, respectively, which are indicated as $\overline{\rho}(s) = \mathrm{Re}[\rho(s)]$ and $\widetilde{\rho}(s) = \mathrm{Im}[\rho(s)]$. The Fisher information matrix is $\Omega = [E(\psi\psi^T)]$, where

$$\boldsymbol{\psi}^T = \frac{\partial Lo}{\partial}\left[\sigma^2 \quad \overline{\rho}^T(1) \quad \widetilde{\rho}^T(1) \quad \cdots \quad \overline{\rho}^T(S) \quad \widetilde{\rho}^T(S) \quad \boldsymbol{\eta}^T\right]. \tag{29}$$

For the Fisher information matrix, the CRB of η conforms,

$$\mathrm{CRB}(\boldsymbol{\eta}) = \frac{\sigma^2}{2}\left\{\sum_{s=1}^{S}\mathrm{Re}\left[\mathbf{F}^H(s)\mathbf{B}^H\mathbf{P}_A^{\perp}\mathbf{B}\mathbf{F}(s)\right]\right\}^{-1}, \tag{30}$$

where

$$\begin{aligned}
&\mathbf{B} = \left[\mathbf{B}_\theta \ \ \mathbf{B}_\varphi \ \ \mathbf{B}_\tau\right],\\
&\mathbf{B}_\theta = \left[\mathbf{b}_{\theta_1} \ \ \mathbf{b}_{\theta_2} \ \cdots \ \mathbf{b}_{\theta_K}\right],\\
&\mathbf{B}_\varphi = \left[\mathbf{b}_{\varphi_1} \ \ \mathbf{b}_{\varphi_2} \ \cdots \ \mathbf{b}_{\varphi_K}\right],\\
&\mathbf{B}_\tau = \left[\mathbf{b}_{\tau_1} \ \ \mathbf{b}_{\tau_2} \ \cdots \ \mathbf{b}_{\tau_K}\right],\\
&\mathbf{b}_{\theta_k} = \left[\frac{\partial\mathbf{A}_k^T}{\partial\theta_k}\right]^T, \mathbf{b}_{\varphi_k} = \left[\frac{\partial\mathbf{A}_k^T}{\partial\varphi_k}\right]^T, \mathbf{b}_{\tau_k} = \left[\frac{\partial\mathbf{A}_k^T}{\partial\tau_k}\right]^T,\\
&\mathbf{A} = \left[\mathbf{A}_1 \ \ \mathbf{A}_2 \ \cdots \ \mathbf{A}_K\right],\\
&\mathbf{P}_A^{\perp} = \mathbf{I} - \mathbf{P}_A = \mathbf{I} - \mathbf{A}\left(\mathbf{A}^H\mathbf{A}\right)^{-1}\mathbf{A}^H,\\
&\mathbf{F}(s) = \mathbf{I}\otimes\mathrm{diag}(\boldsymbol{\rho}(s)).
\end{aligned} \tag{31}$$

We perform simulations using OFDM signals with $L = 64$ subcarriers, fast Fourier transform period $T_{\mathrm{FFT}} = 32$us, carrier frequency $f_c = 2.4$GHz , and bandwidth $B = 20$MHz. Used UPA contains 4×4 array sensors. We set the spectrum steps of $\Delta\tau = 0.001$ns and $\Delta\theta = 0.05^\circ$. For evaluating the precision of the methods, we calculate the root mean square error (RMSE) by the following equation:

$$\mathrm{RMSE} = \sqrt{\frac{1}{QL}\sum_{q=1}^{Q}\left\|\lambda - \widehat{\lambda}_i\right\|^2}, \tag{32}$$

where Q, $\widehat{\lambda}_i$, and λ_i are the amount of Monte Carlo simulations, the estimated values, and the ith true values, separately.

Table 3: Computational complexity comparison.

Algorithm	Complexity
Proposed	$\mathcal{O}(M^4(SL+2^NK)+NK^3+M^2(M^2-K)(G_\varphi G_\theta+G_\tau))$
Vector-based	$\mathcal{O}((SL+M^2)M^4+M^2(M^2-K)G_\varphi G_\theta G_\tau)$
EX-proposed	$\mathcal{O}(M^4L(S+2^NKL)+NK^3+M^2L(M^2L-K)(G_\varphi G_\theta+G_\tau))$
EX-vector-based	$\mathcal{O}((S+M^2L)M^4L^2+M^2L(M^2L-K)G_\varphi G_\theta G_\tau)$

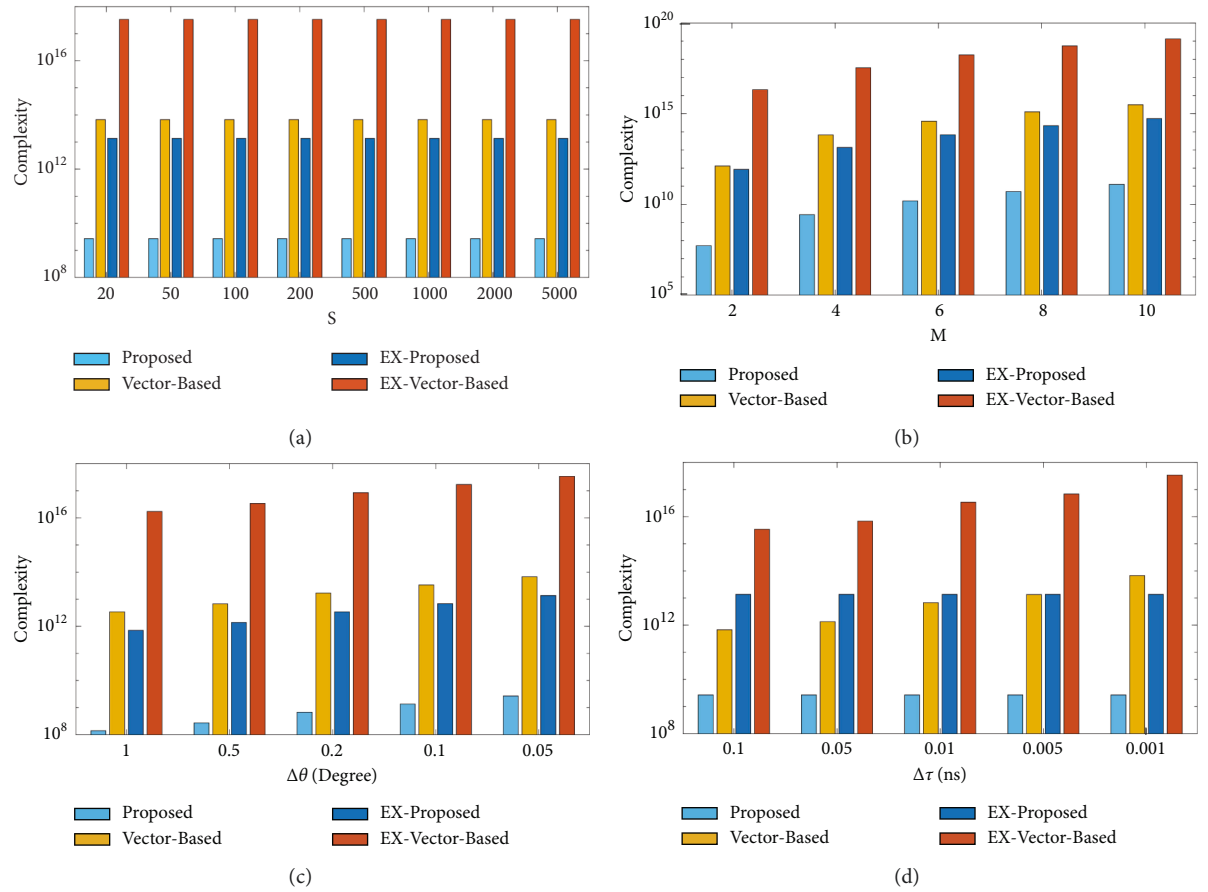

Figure 2: Complexity comparison(a) versus S where $M = 4$, $\Delta\theta = 0.05^\circ$, and $\Delta\tau = 0.001$ns(b)versus M where $S = 500$, $\Delta\theta = 0.05^\circ$, and $\Delta\tau = 0.001$ns(c)versus $\Delta\theta$ where $M = 4$, $S = 500$, and $\Delta\tau = 0.001$ns(d)versus $\Delta\tau$ where $M = 4$, $S = 500$, and $\Delta\theta = 0.05^\circ$.

5.1. Performance at Low Signal-to-Noise Ratio (SNR). Assume that the quantity of multipath is three, the associated delays are 3.5ns, 13.5ns, and 23.5ns, related azimuth angles are -20°, 0° and 30°, and related elevation angle are 20°, 30°, and 45°, separately. Furthermore, $Q = 200$ is chosen and the distribution of TD and AOA under $S = 500$ and SNR = -5dB is determined, as illustrated in Figure 3.

Figure 3 indicates that the proposed algorithm (EX-Proposed) is successful in solving the parameters and the estimated values are concentrated surrounding the true values. Furthermore, the proposed algorithm performs effectively in low SNR.

5.2. Performance versus SNR. This part analyzes the capabilities of EX-Proposed, EX-Vector-Based, Proposed, Vector-Based, and CRB under multipath component conditions. Suppose the multipath components are three with the same parameters as those simulated in A. We choose $Q = 200$, $S = 500$ and the spectrum steps of $\Delta\tau = 0.001$ns and $\Delta\varphi = \Delta\theta = 0.05^\circ$. In addition, the RMSE performance versus SNR, with ranges of -15dB to 20dB in 5dB intervals, as illustrated in Figure 4.

Besides, Figure 4 indicates that the RMSEs of both EX-Proposed and EX-Vector-Based are much higher than those of Proposed and Vector-Based using the single-frequency model. The reason is that both algorithms extend the channel frequency response by combining space-time characteristics from the vector basis and tensor basis, separately. Therefore, the algorithms based on the EX-Response model have higher estimation accuracy and are closer to the CRB than the corresponding single-frequency algorithms.

However, the RMSEs of the tensor-based algorithms (EX-Proposed and Proposed) are both slightly higher than those of the corresponding vector-based algorithms (EX-Vector-Based and Vector-Based). This is due to the CPD

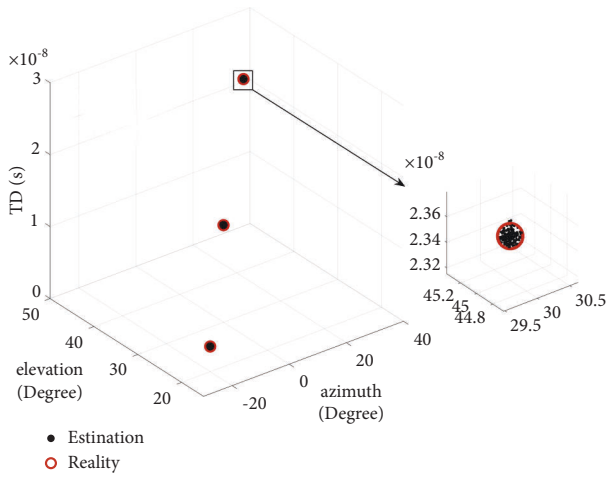

Figure 3: Estimated distribution at SNR = −5dB.

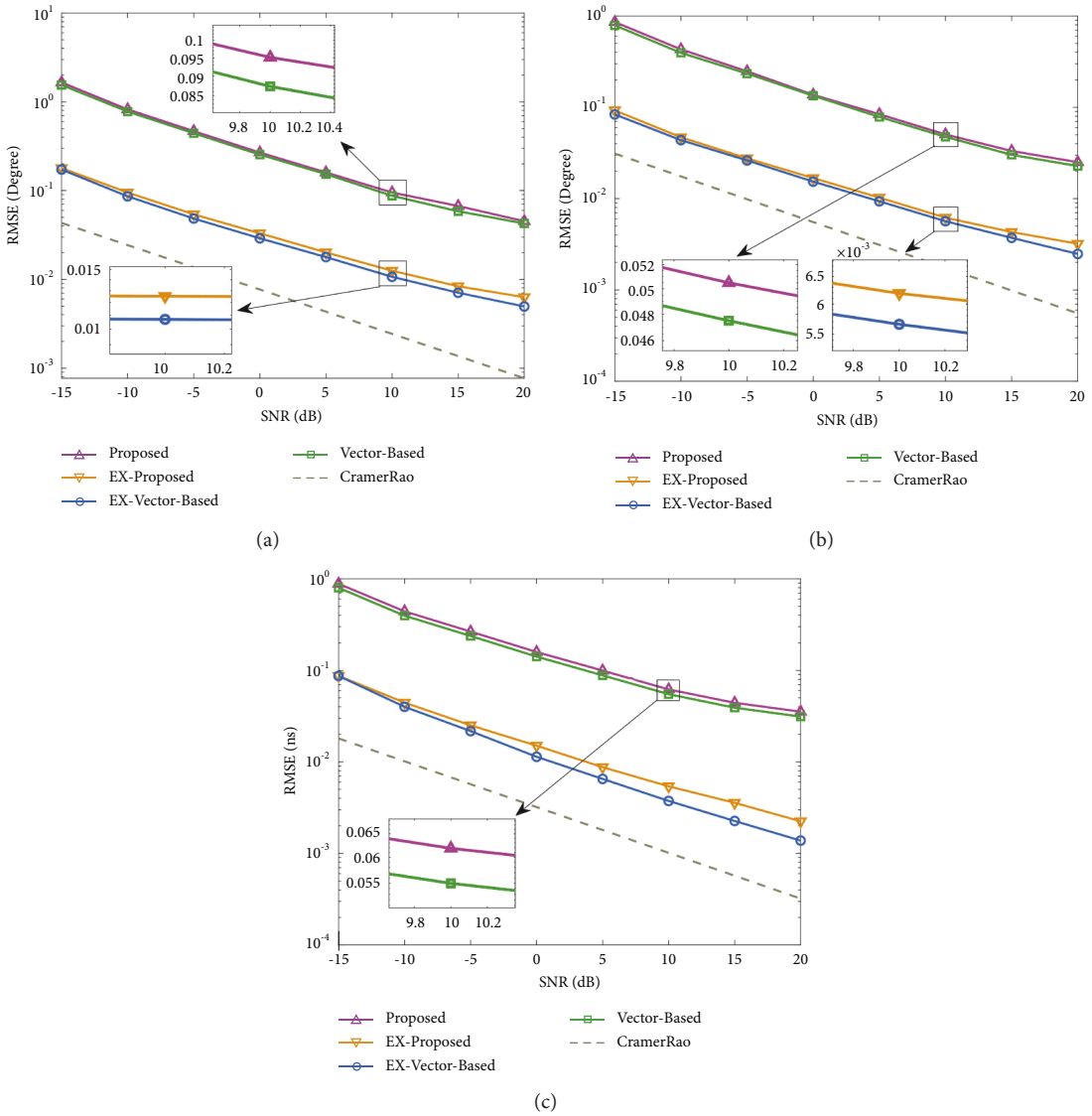

Figure 4: Performance comparison versus SNR: (a) azimuth; (b) elevation; (c) TD.

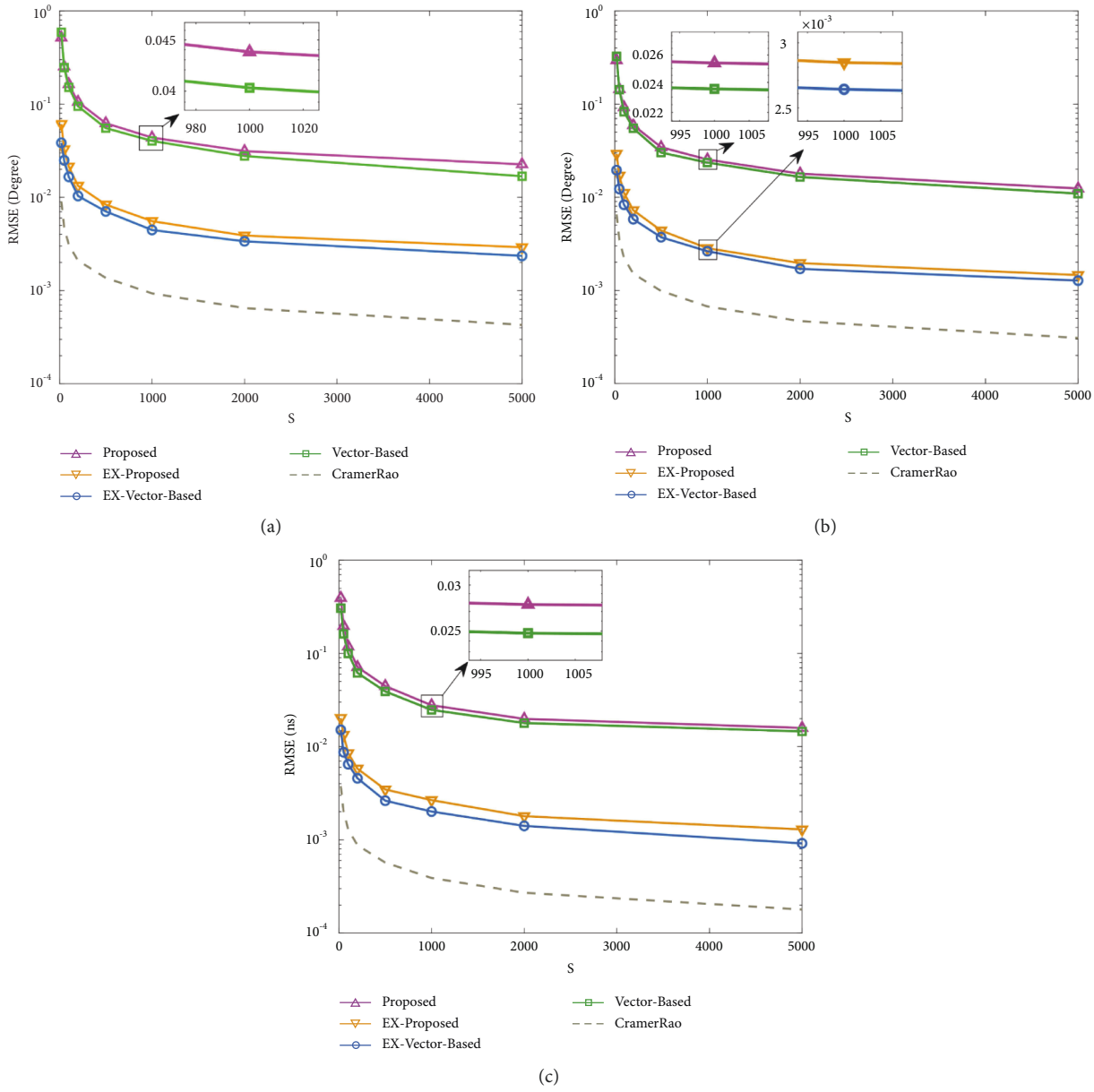

Figure 5: Performance comparison versus snapshots: (a) azimuth; (b) elevation; (c) TD.

process (31) of the tensor algorithm is an approximate operation and the decomposition process has a partial loss of virtual aperture and virtual bandwidth, but its estimation is still accurate. When comparing the complexities, the complexities of EX-Proposed and EX-Vector-Based are about $\mathcal{O}(1.39 \times 10^{13})$ and $\mathcal{O}(3.39 \times 10^{17})$, respectively. Therefore, the proposed algorithm (EX-Proposed) not only obtains a value estimated with high accuracy but also decreases the complexity considerably.

5.3. Performance versus Snapshots. To highlight the impact of snapshots on RMSE, we set SNR = 15dB, the quantity of snapshots varies within the range of $S = \{20, 50, 100, 200, 500, 1000, 2000, 5000\}$, and the rest of the simulation parameters are identical to those simulated in B. As illustrated in Figure 5, the RMSE also decreases along with the increases in the number of snapshots, but the declines are gradually plateauing. The rest of the results are the identical to corresponding simulated in B. The RMSE of the proposed tensor-based algorithm (EX-Proposed) is higher than that of the single-frequency model algorithms (Proposed and Vector-Based), close to that of the vector-based algorithm using the EX-Response model (EX-Vector-Based), while the complexity is much lower.

6. Conclusions

For joint estimation of TD and AOA at UPA and solving the problem of high computational complexity, we propose a fast joint estimation algorithm using tensor structures and OFDM techniques. Furthermore, we combine the receive

antenna array response and the channel frequency response of OFDM subcarriers through a tensor structure to obtain more useable information with less complexity. In summary, the signal model and the algorithmic process under vector and tensor structures are first explained, from which we interpret the correspondence between the two structures. The related algorithms are then analyzed for their complexity, which demonstrates the relative advantage of the proposed method. Lastly, the simulation results illustrate that the proposed algorithm is considerably less complex than the conventional vector-based algorithm while maintaining a higher estimation accuracy.

In the future, we will further exploit the dimensionality reduction advantage of the proposed algorithm to explore more algorithms that can match the model, such as spatial smoothing methods [24], which can increase the robustness under coherent multipath conditions. Moreover, the applicability of the tensor structure on the proposed model fully illustrates its structural advantages and greatly extends the possibilities of the joint estimation algorithm.

Data Availability

The authors claim that the data used in this paper are provided by our simulations and that the material used to support the findings of this study is available from the corresponding author on request.

Conflicts of Interest

The authors declare that they have no conflict of interest.

References

[1] A. Sahin, R. Yang, M. Ghosh, and R. L. Olesen, "An Improved Unique Word Dft-Spread Ofdm Scheme for 5g Systems," in *Proceedings of the 2015 IEEE Globecom Workshops (GC Wkshps)*, pp. 1–6, IEEE, San Diego, CA, USA, December 2015.

[2] C. Ball, E. Humburg, K. Ivanov, and F. Treml, "Performance analysis of ieee802. 16 based cellular man with ofdm-256 in mobile scenarios,"vol. 3, pp. 2061–2066, in *Proceedings of the 2005 IEEE 61st Vehicular Technology Conference*, vol. 3, IEEE, Stockholm, Sweden, May 2005.

[3] L. Wang and B. Jezek, "Ofdm modulation schemes for military satellite communications," in *Proceedings of the MILCOM 2008-2008 IEEE Military Communications Conference*, pp. 1–7, IEEE, San Diego, CA, USA, November 2008.

[4] B. Turan, O. Narmanlioglu, S. C. Ergen, and M. Uysal, "On the performance of mimo ofdm-based intra-vehicular vlc networks," in *Proceedings of the 2016 IEEE 84th Vehicular Technology Conference (VTC-Fall)*, pp. 1–5, IEEE, Montreal, QC, Canada, September 2016.

[5] Y.-X. Guo, X.-A. Song, R.-Q. Zhang, and H. Li, "Research on underwater acoustic communication system based on ofdm-oam," *Automatic Control and Computer Sciences*, vol. 54, no. 6, pp. 541–548, 2020.

[6] Y. Zheng, M. Sheng, J. Liu, and J. Li, "Exploiting aoa estimation accuracy for indoor localization: a weighted aoa-based approach," *IEEE Wireless Communications Letters*, vol. 8, no. 1, pp. 65–68, 2019.

[7] S. Kim, B. Kim, and J. Lee, "Low-complexity-based rd-music with extrapolation for joint toa and doa at automotive fmcw radar systems," *Journal of Sensors*, vol. 2020, Article ID 7342385, 13 pages, 2020.

[8] F. Cao and M. Li, "Frequency domain doa estimation and tracking of uwb signals," in *Proceedings of the 2010 6th International Conference on Wireless Communications Networking and Mobile Computing (WiCOM)*, September 2010.

[9] H. Ni, G. Ren, and Y. Chang, "Novel toa estimation algorithm for ofdm wireless networks," *Journal of Xidian University*, vol. 36, no. 1, pp. 17–21, 2009.

[10] J. Wang and Z. Shen, "An improved music toa estimator for rfid positioning," in *Proceedings of the 2002 International Radar Conference*, pp. 478–482, Edinburgh, UK, October 2002.

[11] S. Kim, D. Oh, and J. Lee, "Joint dft-esprit estimation for toa and doa in vehicle fmcw radars," *IEEE Antennas and Wireless Propagation Letters*, vol. 14, pp. 1710–1713, 2015.

[12] H. Jiang, F. Cao, and R. Ding, "Propagator method-based toa estimation for uwb indoor environment in the presence of correlated fading amplitudes," in *Proceedings of the 2008 4th IEEE International Conference on Circuits and Systems for Communications*, pp. 535–538, IEEE, Shanghai, China, May 2008.

[13] Q. Shen, W. Liu, W. Cui, and S. Wu, "Low-complexity compressive sensing based doa estimation for co-prime arrays," in *Proceedings of the 2014 19th International Conference on Digital Signal Processing*, pp. 754–758, IEEE, Hong Kong, China, August 2014.

[14] R. Ding, Z. H. Qian, and X. Wang, "Uwb positioning system based on joint toa and doa estimation," *Journal of Electronics and Information Technology*, vol. 32, no. 2, pp. 313–317, 2010.

[15] H. Xu, Y. Zhang, B. Ba, D. Wang, and X. Li, "Fast joint estimation of time of arrival and angle of arrival in complex multipath environment using ofdm," *Institute of Electrical and Electronics Engineers Access*, vol. 6, pp. 60613–60621, 2018.

[16] N. D. Sidiropoulos, L. De Lathauwer, X. Fu, K. Huang, E. E. Papalexakis, and C. Faloutsos, "Tensor decomposition for signal processing and machine learning," *IEEE Transactions on Signal Processing*, vol. 65, no. 13, pp. 3551–3582, 2017.

[17] R. Zhao, Q. Wang, J. Fu, and L. Ren, "Exploiting block-sparsity for hyperspectral kronecker compressive sensing: a tensor-based bayesian method," *IEEE Transactions on Image Processing*, vol. 29, pp. 1654–1668, 2020.

[18] H. Chen, F. Ahmad, S. Vorobyov, and F. Porikli, "Tensor decompositions in wireless communications and mimo radar," *IEEE Journal of Selected Topics in Signal Processing*, vol. 15, no. 3, pp. 438–453, 2021.

[19] K. Luo, X. Zhou, B. Wang, J. Huang, and H. Liu, "Sparse bayes tensor and doa tracking inspired channel estimation for v2x millimeter wave massive mimo system," *Sensors*, vol. 21, no. 12, p. 4021, 2021.

[20] W. Jhang, S.-W. Chen, and A.-C. Chang, "Computationally efficient doa estimation for massive uniform linear array," *IEICE - Transactions on Fundamentals of Electronics, Communications and Computer Sciences*, vol. E103.A, no. 1, pp. 361–365, 2020.

[21] H. Zheng, C. Zhou, Y. Gu, and Z. Shi, "Two-dimensional doa estimation for coprime planar array: a coarray tensor-based solution," in *Proceedings of the ICASSP 2020-2020 IEEE International Conference on Acoustics, Speech and Signal Processing (ICASSP)*, pp. 4562–4566, IEEE, Barcelona, Spain, May 2020.

[22] T. G. Kolda and B. W. Bader, "Tensor decompositions and applications," *Society for industrial and applied mathematics Review*, vol. 51, no. 3, pp. 455–500, 2009.

[23] P. Stoica and A. Nehorai, "Music, maximum likelihood, and cramer-rao bound," *IEEE Transactions on Acoustics, Speech, & Signal Processing*, vol. 37, no. 5, pp. 720–741, 1989.

[24] M. Xiao, Z. Duan, and Z. Yang, "A weighted forward-backward spatial smoothing doa estimation algorithm based on tls-esprit," *IEICE - Transactions on Info and Systems*, vol. E104.D, no. 6, pp. 881–884, 2021.